Cell wall thickness has phylogenetically consistent effects on photosynthetic N-use efficiency of land species

Dan-dan Liu[1†], Tiina Tosens[2], Dong-liang Xiong[3], Marc Carriquí[4], You-cai Xiong[1], Wei Xue[1*,†]

[1]College of Ecology, State Key Laboratory of Grassland Agroecosystems, Lanzhou University, Lanzhou 730000, China

[2]Institute of Agricultural and Environmental Sciences, Estonian University of Life Sciences, Kreutzwaldi, Tartu 51014, Estonia

[3]National Key Laboratory of Crop Genetic Improvement, Hubei Hongshan Laboratory, MOA Key Laboratory of Crop Ecophysiology and Farming System in the Middle Reaches of the Yangtze River, Huazhong Agricultural University, Wuhan 430070, China

[4]Research Group on Plant Biology under Mediterranean Conditions, Institut d'Investigacions Agroambientals i d'Economia de l'Aigua (INAGEA) – Universitat de les Illes Balears (UIB), Ctra Valldemossa Km 7.5., 07122, Illes Balears, Spain

*Corresponding author: Wei Xue. E-mail: xuewei@lzu.edu.cn, Tel: 0931-8915950

†These authors contributed equally to this work

Current address for Wei Xue: Lanzhou University, No.222 Tianshui South Road, Lanzhou, China

Abstract Photosynthetic nitrogen-use efficiency (PNUE) varied greatly among C_3 species. However, morpho-physiological mechanisms and interrelationships shaping PNUE remain unclear at an evolutionary time scale. Here, we compiled a novel large matrix of leaf morpho-anatomical and physiological traits in 679 C_3 species from bryophytes to angiosperm to further understand the complexity of interrelationships underlying PNUE variations. We found that LMA, mesophyll cell wall thickness (T_{cwm}), Rubisco N allocation fraction (P_R), and mesophyll conductance (g_m) together interpreted 83% of PNUE variations, 65% of which were explained by P_R and g_m. However, the P_R effects were species-dependent on g_m; that is, the P_R contribution on PNUE was massively greater in high-g_m species than that in low-g_m ones. Paired-trait correlation analysis and path analysis indicated a weak correlation between PNUE and LMA, while the paired PNUE–T_{cwm} correlation was strong. The P_R was inversely proportional to T_{cwm} which was similar to the g_m–T_{cwm} relationship ($p < 0.01$), so that the internal CO_2 drawdown from intercellular airspace to carboxylaton sites was relatively conservative over a wide range of T_{cwm}. Collectively, coordinated changes in P_R and g_m connecting T_{cwm} suggested the T_{cwm}-mediated complex physiology mechanisms controlling the PNUE across contrasting plant groups.

Keywords: photosynthetic nitrogen-use efficiency, nitrogen allocation, mesophyll conductance, cell wall thickness, leaf mass per area

Introduction

Photosynthetic nitrogen-use efficiency (PNUE) is defined as the ratio of light-saturated photosynthesis to leaf nitrogen content, being a core process of the leaf economics spectrum (LES) (Wright *et al*., 2005). Considerable variations in the PNUE economic trait were observed. There is a correlation between PNUE and LMA in spermatophyta: species with high LMA almost invariably have low PNUE (Reich *et al*., 1998; Wright *et al*., 2005; Onoda *et al*., 2017). The LMA, as a complex leaf morphologic trait, cannot explain inter-specific PNUE variations (Shipley *et al*., 2006; Warren and Adams, 2006; Hidaka and Kitayama, 2009; Onoda *et al*., 2017; Flexas and Carriquí, 2020; Luo *et al*., 2021). Given the ecological significance of the inter-specific variations of PNUE with respect to relative growth rate and crop yield or for a sake of realistic ecosystem modeling (Poorter *et al*., 1990; Garnier *et al*., 1995; Reich *et al*., 1998; Oguchi *et al*., 2016; Yin *et al*., 2019), morpho-physiological mechanisms and interrelationships underlying the PNUE are attracting ever-increasing.

Previous studies suggested that variations in PNUE resulted from interactive mechanisms of several foliage physiological and anatomical traits (Hikosaka, 2004, 2010; Wright *et al*., 2005; Onoda *et al*., 2017; Flexas and Carriquí, 2020). In particular, nitrogen allocation into photosynthetic apparatus and mesophyll conductance for internal CO_2 diffusion (g_m) were important. Experimental studies observed an inverse proportion phenomenon between LMA and the fraction of nitrogen allocated to photosynthetic proteins in spermatophyta. With increasing LMA in ten dicotyledonous species, photosynthetic N allocation fraction declined from 50% to 38%, with a large decline in the Rubisco N allocation fraction (P_R) (Poorter and Evans, 1998). Hikosaka *et al*. (1998) analyzed an annual herb and an evergreen tree, reporting a higher P_R of 23.2% in the low-LMA herb than the high-LMA tree. Similar results were also observed in other studies that the high-LMA species and genotypes had a smaller P_R (Warren and Adams, 2000; Ripullone *et al*., 2003; Onoda *et al*., 2004; Pons and Westbeek, 2004; Takashima *et al*., 2004; Onoda *et al*., 2017; Gvozdevaite *et al*., 2018; Lei *et al*., 2021a). A meta-analysis in spermatophyta by Onoda *et al*. (2017) attributed the negative PNUE–LMA relationship to trade-off mechanisms between photosynthesis and structural persistence (hereinafter called LMA-mediated function-structure tradeoff in spermatophyta), namely, species at the high-end of the LMA axis were prone to preserve a greater fraction of leaf nitrogen in

structural tissues and thus had lower P_R and PNUE. The PNUE variation from the low-end LMA axis to the high-end was related to increased N investments in structural tissue. Recently, a study quantifying a negative P_R–LMA relationship in spermatophyta has supported it (Luo *et al*., 2021).

An inevitable result of the construction cost for structural tissues is a reduction in g_m (Onoda *et al*., 2017; Flexas and Carriquí, 2020), with a declining tendency in g_m from the low-end of the LMA axis to the high-end in spermatophyta. In ferns and mosses, the observed PNUE variations were strongly associated with g_m (Tosens *et al*., 2016; Carriquí *et al*., 2019). Ferns and mosses with similar low LMA as seed plants had substantially lower g_m and PNUE as compared to the seed plants at the low-end of the LMA axis (Carriquí *et al*., 2015; Tosens *et al*., 2016), which indeed contradicted the negative PNUE–LMA pattern on which the LMA-based function-structure tradeoff opinion was dependent. Contrasting to critical roles of g_m in PNUE in mosses and ferns, several studies in seed plants found that g_m did not contribute to PNUE variations in 11 evergreen tropical and temperate species that differed in LMA (Bahar *et al*., 2018) and in 26 wild and 31 domesticated cotton genotypes with large variations in LMA (Lei *et al*., 2021b). It suggested that the LMA-based function-structure tradeoff framework in spermatophyta developed by Onoda *et al*. (2017) may have a limited capability of addressing the underpinnings of PNUE variations across land plant's phylogeny. Bryophytes and pteridophytes are important from an evolutionary point of view due to their pioneering positions in the land transition of photosynthetic life, and now attracting a considerable attention among researchers due to their great potential in biotechnology and bioindication (Preston and Hill, 1999; Popper and Fry, 2003; Wang *et al*., 2013; Gago *et al*., 2019; Flexas and Carriquí, 2020). Hence, clarifying the roles of LMA in PNUE variations, its correlations with g_m and P_R as well as g_m and P_R functioning mechanisms across major plant groups and phylogenetic interrelationships was of high priority to better understand PNUE variations at an evolutionary time scale.

The g_m is a highly complex trait with a strong sensitivity to leaf anatomy and biochemical traits mediating liquid phase diffusion (e.g., effective porosity of the cell wall-p_i, the CO_2 permeability of membranes, carbonic anhydrase activity) (Evans *et al*., 2009; Kaldenhoff, 2012; Tosens *et al*., 2012; Han *et al*., 2018; Gago *et al*., 2019; Carriquí *et al*., 2020; Evans, 2021; Flexas *et al*., 2021), which compound efforts to scale PNUE with g_m (Warren and Adams, 2006). Pleiotropic compensatory changes

(e.g., one advantageous factor compensates for another drawback) may exert distinct roles when comparing PNUE in a few species or in species that occupy the same habitat in which resource use strategies tend to converge (Evans *et al*., 2009; Anderegg *et al*., 2018; Lei *et al*., 2021b; Nadal *et al*., 2021). In order to elucidate mechanisms of PNUE variations at an evolutionary time scale, a new unprecedented global database was compiled, including leaf morphological, anatomical, and physiological traits of terrestrial C_3 species from bryophytes to angiosperm. Data in C_4 species that have different photosynthetic mechanisms from the C_3 species were not the major concern in this study. Data analysis and presentation in *Results* section were conducted within major taxonomic group (i.e., bryophytes, pteridophytes, gymnosperm, and angiosperm) and across taxonomic groups, helping clarify the scales at which our results were applicable. Specifically, we aimed to address three questions as follows:

(1) What is the evolutionary pattern of PNUE from bryophytes to angiosperm? Are PNUE variations across major taxonomic groups primarily associated with LMA?

(2) What are the important morpho-anatomical factors in shaping PNUE variations across major taxonomic groups?

(3) What are the interrelationships between these important morpho-anatomical factors and PNUE across major taxonomic groups?

Materials and Methods

Data collection

In this study, we constructed a global dataset of leaf morphological, anatomical, and physiological traits of non-stressed mature leaves of terrestrial C_3 species covering major plant groups and phylogeny. The dataset includes the photosynthetic organs with variable morphologies (e.g. phyllidia or thalli in mosses and lichen species). Leaf structural and anatomical traits included LMA and leaf thickness (T_{leaf}), chloroplast surface area exposed to intercellular airspace per unit leaf area (S_c), mesophyll surface area exposed to intercellular airspace per unit leaf area (S_m), cytoplasm thickness (T_{cyt}), mesophyll cell wall thickness (T_{cwm}), mesophyll thickness (T_{mes}), chloroplast thickness (T_{chl}), the fraction of intercellular air space (f_{ias}), the average distance between the chloroplast and the cell wall (cytoplasm thickness, L_{ct}). Physiological traits consisted of photosynthetic capacity at normal atmospheric CO_2 concentration and saturation light (A_{mass}, mass-based photosynthesis rate), leaf

nitrogen content per leaf mass (N_{mass}), stomatal conductance to water vapor (g_{sw}), intercellular and chloroplastic CO_2 concentration (C_i and C_c, respectively), g_m, the maximum carboxylation rate (V_{cmax}), the maximum electron transport rate (J_{max}), stomatal limitation on photosynthesis (l_s), mesophyll limitation on photosynthesis (l_m), biochemical limitation on photosynthesis (l_b), and leaf temperature (L_{temp}). Papers that highlighted "mesophyll conductance" or "internal conductance" keywords archived by the Web of Science (https://www.webofscience.com) and the China National Knowledge Infrastructure (https://www.cnki.net) until July 2022 were considered in this study. Trait measurements in most species including ferns and moss species in the field and/or outdoor conditions when their growth conditions were most favorable (i.e. with least environmental stress) were regarded as reliable for use. Measurements in shade-adapted leaves within plant canopies were not considered in the global dataset.

The data collection campaign was challenged because the number of available traits differed among surveyed papers. If the traits can be inferred by supporting information, the inferred values were replenished to the global database. In fact, it is not possible to determine the CO_2 concentration within the chloroplast stroma. Hence, the internal CO_2 drawdown (DeltaC, the difference between C_i and C_c) was inferred according to the Fick's first law: DeltaC = $C_a - A(1.56/g_{sw} - 1/g_m)$, which was commonly adopted in leaf photosynthesis-stomatal conductance coupled model (Onoda *et al*., 2017; Xue *et al*., 2022). Bryophytes are the only group of plants that are entirely devoid of stomata. Hence, the DeltaC values in bryophytes species were inferred by the equation of DeltaC = A/g_m. The global C_a of 380 ppm was applied in condition of absent C_a data in surveyed papers.

The P_R was calculated by using two different methods: the numerical calculation method using V_{cmax} and N_{area} as shown by Niinemets and Tenhunen (1997), and the chemical assay in Rubisco content. In most surveyed papers, the Sharkey online calculator (Sharkey *et al*., 2007) and optimization inversion algorithms such as the Bayesian algorithm were two common methods to estimate the C_c-based V_{cmax} from the A/C_i curve (Xue *et al*., 2022). The estimated V_{cmax} values were comparable among plant species, since Rubisco kinetics parameters incorporated in the parameter estimation methods were consistently taken from the study of Bernacchi *et al*. (2002). Variation in Rubisco kinetics parameters measured *in vitro* was less than 10% among C_3 plant species (von Caemmerer, 2020), which was far less than the 10-fold

variations of inter-specific A_{mass} at a given LMA (Fig. 1d). Hence, their Rubisco kinetics parameters may be highly recommended for V_{cmax} calculations across major plant functional types, as commonly did in previous studies. The P_R dataset inferred from the chemical assay in the study of Onoda *et al*. (2017) was solely limited to spermatophyte. The P_R chemical assay dataset was expanded to include the P_R numerical calculations to enrich species diversity in the global dataset. All leaf trait data in the global database were measured in sunlit leaves under relatively high incident radiation and ambient atmospheric CO_2 concentration at around 25°C. The P_R estimations by the numerical method were sensitive to measuring temperatures (Niinemets and Tenhunen, 1997). V_{cmax} and J_{max} measured at other leaf temperatures were converted to values at standard temperature 25°C using temperature response functions of V_{cmax} and J_{max} with activation energy (ΔH_a) at 63.0 kJ mol^{-1} according to Medlyn *et al.* (2002).

Except for the DeltaC and P_R, other physiological and morpho-anatomical traits' values were directly taken from the surveyed papers. Leaf trait data of the same species reported by different studies were averaged for use when environmental conditions sensed by the species were optimal to avoid any effect of environmental stress on analysis (Poorter *et al*., 2009; Poorter *et al*., 2011; Xing *et al*., 2021). Wild, old and modern crop kinds differed greatly in leaf morpho-physiological traits, being representatives of angiosperm species in the leaf economics spectrum evolving towards higher photosynthetic efficiency (Xiong and Flexas, 2018; Martin *et al*., 2018; Hayes *et al*., 2019). In such case, physiological and morpho-anatomical traits in crops and non-crop plants were merged for data analysis. In total, there were 1296 lines of data in 679 species, covering major life forms in land plants including bryophytes (57 lines in mosses and lichen species), pteridophytes (64 lines in ferns and fern allies species), gymnosperm (83 lines in needles and scales leaved species), and angiosperm (1092 lines in trees, shrubs, grass and crops).

Data analysis

Because data types of some leaf traits were not a normal distribution, data of all traits were $\log_{10}$-transformed before correlation analysis, which was a common practice adopted in ecological studies (Wright *et al*., 2005; Carriquí *et al*., 2015; Tosens *et al*., 2016; Onoda *et al*., 2017; Carriquí *et al*., 2019). The standardized major axis slope (SMA, also known as reduced major axis slopes), a common practice seen

in these studies, was applied to determine the strength of bivariate trait correlation. For paired traits with significant curvilinear relationship, rise to the maximum or decline to the minimum curve trajectory was predicted by the non-parametric regression model (locally weighted regression, Loess) following Xue *et al*. (2021) and Kurmangozhinov *et al*. (2020), aiming to clarify threshold at which trait strong coupling shifted to weak coupling. Indeed, it is the mass-based physiological traits such as A_{mass} that characterize the biochemical capacity of single cells and are the key players in the worldwide trade-off between the physiological and structural characteristics of foliage (Niinemets and Tenhunen, 1997; Wright *et al*., 2005; Tosens *et al*., 2016; Onoda *et al*., 2017). We found that the area-based trait analysis showed analogous results in correlation analysis as the mass-based trait expression. Hereinafter, the mass-based physiological traits were used for correlation analysis unless otherwise indicated. Before paired trait correlation analysis, we constructed a phylogenetic tree for all species using the megatree approach in the R package V.PHYLOMAKER and estimated the phylogenetic signals using the Pagel's λ following Xing *et al.* (2021). There were 39 species failing to be bound to the constructed phylogenetic tree because they were not present in the plantlist database of the V.PHYLOMAKER package (package acquiring date: 2022/05/13). Of the 39 species, one was *Polistichium aculeatum* (pteridophyte) and the rest belonged to the bryophyte.

The paired-trait correlation analysis using the smatr package, Loess model application, and phylogenetic signal analysis using the V.PHYLOMAKER package was conducted in R 4.0.5 software (R Core Team, 2021). To explore how morpho-physiological traits influence PNUE variations, structural equation modeling (SEM) was applied (Shipley, 2004). The estimator to parameterize the SEM was the maximum likelihood method. Appropriate SEM model fit was inspected by the comparative fit index (CFI, > 0.9), p-value, and the standard root mean squared residual (SRMR, < 0.08) (Shipley, 2004). The SEM analysis was conducted using the lavaan package (Rosseel, 2012) and visualized using the semPlot package in the R software.

The relative importance of P_R and g_m in relation to PNUE variations was quantified by the photosynthetic coordination theory. According to the biochemical photosynthesis model established by Farquhar *et al*. (1980), the photosynthetic rate is limited by either the Rubisco carboxylation rate at low Rubisco content and CO_2

concentrations (A_c) or the RuBP regeneration rate at relatively high CO_2 concentrations due to low electron transport rates (A_j). At a given leaf temperature, the A_c value is primarily determined by V_{cmax}, followed by C_c (Eqn 1). Different from the direct impacts of the P_R on photosynthesis, g_m effects on photosynthesis were achieved through its impacts on C_c (Ethier & Livingston, 2004; Evans *et al*., 2009; Kaldenhoff, 2012; Tosens *et al*., 2012; Onoda *et al*., 2017; Gómez-Ocampo *et al*., 2021). The photosynthetic coordination theory originally proposed by von Caemmerer and Farquhar (1981) and further developed by Maire *et al.* (2012) in 31 individual C_3 species, Wang *et al*. (2017), Smith *et al*. (2019), and Harrison *et al*. (2021) in regional vegetation studies states that photosynthesis tends to be co-limited by electron transport and carboxylation under average environmental conditions, thus maximizing potential resource use for growth and reproduction. The photosynthetic coordination theory provides a quantitative approach to predicting P_R and g_m functioning effects on inters-pecific PNUE variations. The PNUE can be expressed with Eqn 3 that was inferred from Eqn 1 and Eqn 2 as follows:

$$A_{area} = \left(1 - \frac{\Gamma^*}{C_c}\right) A_c - R_d = \left(1 - \frac{\Gamma^*}{C_c}\right) \frac{V_{cmax} C_c}{C_c + K_m} - R_d \quad (1)$$

$$\frac{A_{area}}{N_{area}} = \left(1 - \frac{\Gamma^*}{C_c}\right) \frac{V_{cmax}/N_{area}}{1 + K_m/C_c} - \frac{R_d}{N_{area}} \quad (2)$$

$$PNUE = \left(1 - \frac{\Gamma^*}{C_c}\right) \frac{6.25 V_{cr}}{1 + K_m/C_c} P_R - \frac{R_d}{N_{area}} \quad (3)$$

where V_{cr} is the maximum carboxylation rate per unit Rubisco protein (47.34 μmol CO_2 (g Rubisco)$^{-1}$ s^{-1} at 25°C) and 6.25 is the nitrogen content of Rubisco protein (Niinemets and Tenhunen, 1997; Luo *et al*., 2021); R_d is area-based dark respiration in the light; Γ* is chloroplast CO_2 compensation point, equal to 42.75 μmol mol^{-1} at 25°C. K_m is equal to $K_c(1+O/K_o)$, where K_c and K_o are the Michaelis–Menten constants for CO_2 and O_2, respectively (Bernacchi *et al*., 2002). The PNUE simulations were generated considering a continuous series of P_R and C_c. We anticipated that impacts of g_m on PNUE were more obvious across contrasting plant groups with large differences in g_m than that in several randomly selected species. Hence, the species in the global dataset were divided into two groups according to the g_m values: the high- and low-g_m species assembles. The high-g_m species assemble had g_m values ranging from 0.25 to 0.32 mol m^{-2} s^{-1}, and the low-g_m species assemble had g_m from 0.05 to 0.06 mol m^{-2} s^{-1}, corresponding to C_c at about 100 and 230 μmol mol^{-1} in leaves under current atmospheric CO_2 condition, respectively. The PNUE

and P_R measurements together with g_m and C_c measurements (i.e., trait values taken/inferred from the surveyed papers) in the two species assembles were applied to cross-validate PNUE theoretical predictions. Variations in predicted PNUE were assumed to be not affected by the intercept R_d/N_{area}.

Results

The evolutionary pattern of PNUE and its relationship with LMA

The LMA, PNUE, A_{mass}, N_m, V_{cmax}, J_{max}, P_R, g_m, DeltaC, and T_{cwm} exhibited significant phylogenetic signals (Table S1). Firstly, we mapped the LMA phylogenetic pattern and its relationship with PNUE, A_{mass}, and N_m because LMA was considered a critical factor influencing the PNUE economic trait in seed plants (Hikosaka, 2004; Wright *et al*., 2005; Onoda *et al*., 2017). The mean of LMA cluster data slightly increased from bryophytes to pteridophytes (TukeyHSD, $p = 0.07$) (Fig. 1a). No significant differences in mean LMA were observed between pteridophytes and angiosperm ($p = 0.27$, Fig. 1a). The mean LMA in gymnosperm was significantly higher than in the other three phyla ($p < 0.01$). The ANOVA results in mean PNUE showed significant differences among the four phyla (Fig. 1b), with the highest PNUE found in angiosperm ($p < 0.05$) and similar PNUE values among the other three phyla ($p > 0.1$). Significantly lower PNUE was evident in bryophytes at the same LMA as seed plants, and pteridophyte had slightly lower PNUE (Fig. 1c). The LES SMA regression (fit SMA model to all data in the four phyla) had a low r^2 at 0.1, due to a significant deviation of bryophytes data from the LES SMA regression line (Fig. 1c, SMA ANOVA in intercept: $p < 0.01$). Improved performance in the LES SMA regression for A_{mass}–LMA was evident ($r^2 = 0.33$), whereas all A_{mass} values in bryophytes significantly deviated from the LES SMA regression line primarily due to large differences in intercept (Fig. 1d, SMA ANOVA in intercept: $p < 0.01$). For the N_m–LMA relationship, the LES SMA regression line and the phylum SMA regression lines (fit SMA model to data of each phylum) were close to each other (Fig. 1e), showing a higher $r^2 = 0.53$. It was suggested that PNUE variations through plant phylogeny were weakly associated with LMA primarily due to large discrepancies in slope and intercept of the A_{mass}–LMA relationship among major taxonomic groups.

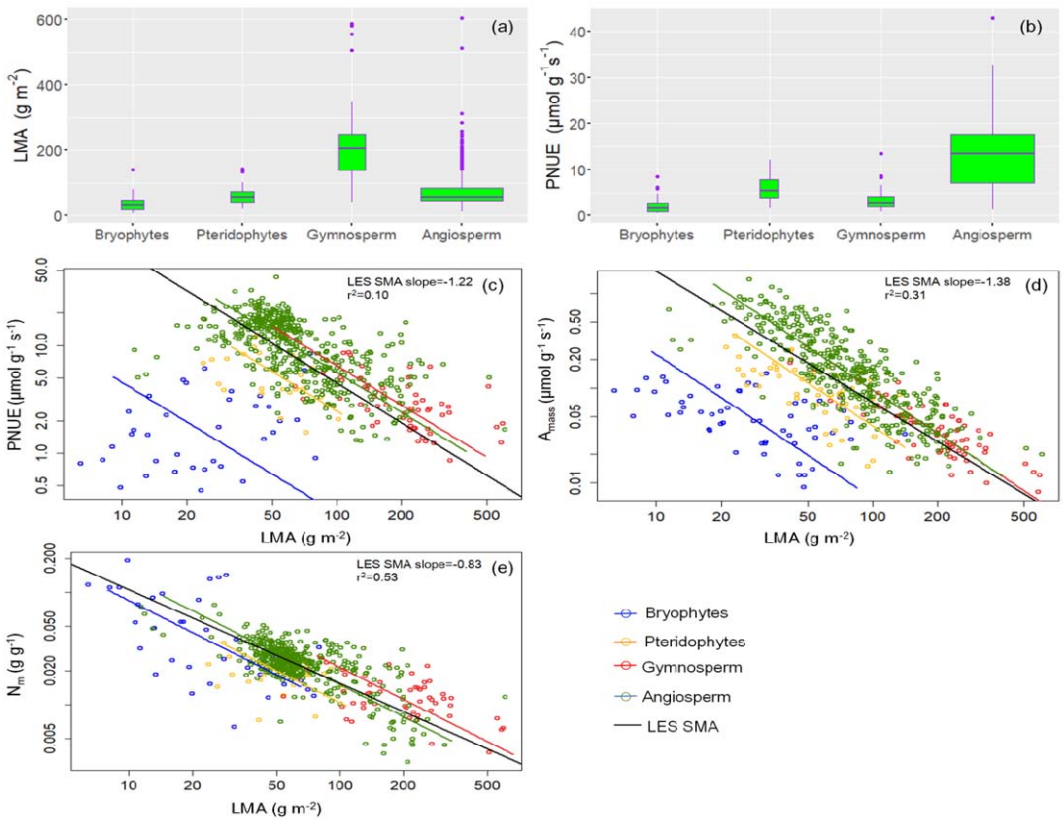

Fig. 1. The phylogenetic patterns of leaf mass per area (LMA, a) and photosynthetic N-use efficiency (PNUE, b), and paired-trait relationships between PNUE, mass-based photosynthesis capacity (A_{mass}), leaf nitrogen content per leaf mass (N_m), and LMA. (c) PNUE–LMA, (d) A_{mass}–LMA, (e) N_m–LMA. The black line was the regression of standard major analysis (SMA) fit to all data in the four phyla (LES SMA) and the other lines were SMA regressions fit to all data of each phylum. The r^2 and slope values were annotated for the LES SMA regression. The boxes were drawn with widths proportional to the square-roots of the number of observations in the phyla. The same symbol legends for bryophytes, pteridophytes, gymnosperm, and angiosperm as Fig. 1 were used in other figures unless otherwise indicated.

Effects of photosynthetic nitrogen allocation and g_m on photosynthesis and PNUE variations

No significant correlation for PNUE–N_m was observed (LES SMA r^2 = 0.002, p = 0.32), while the LES SMA fit for PNUE–A_{mass} had r^2 as high as 0.58 (Fig. S1), suggesting that PNUE changing pattern along the LMA axis was strongly shaped by A_{mass}. Hence, quantitative relationships between key physiological traits and A_{mass} were explored in this paragraph. A positive LES SMA regression line for the A_{mass}–V_{cmax} relationship had r^2 = 0.68, which overlapped the four phylum regression lines well (Fig. 2a, SMA ANOVA in slope: p = 0.07). A closer correlation for the LES SMA regression fit to A_{mass}–g_m was evident with r^2 at 0.74, without showing

significant differences against phylum regression lines (Fig. 2b, SMA ANOVA in slope: p = 0.9). The V_{cmax} was tightly related to J_{max} with r^2 as high as 0.89 (Fig. 2c), close to four phylum regression lines (SMA ANOVA in slope: p = 0.04). The g_m and V_{cmax} relationship featured relatively weaker correlation strength than that for V_{cmax}–J_{max} (r^2 = 0.5, Fig. 2d).

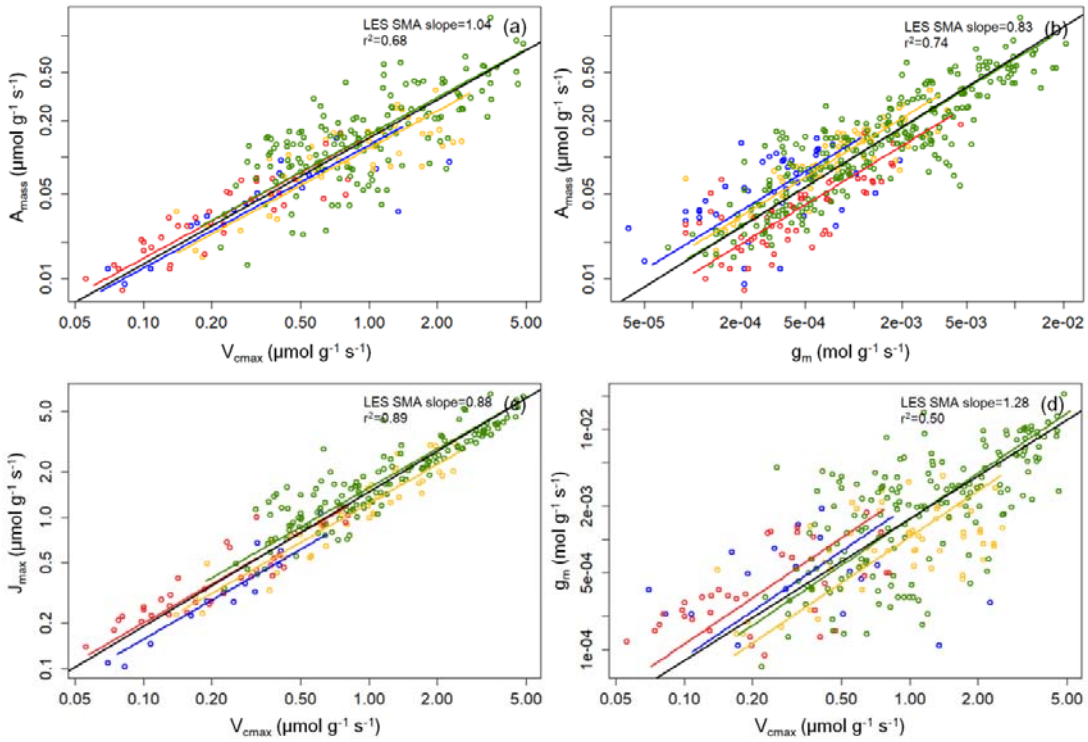

Fig. 2. Paired-trait correaltions between the mass-based photosynthesis (A_{mass}), the mass-based maximum carboxylation rate (V_{cmax}), the mass-based mesophyll conductance (g_m), and the mass-based maximum electron transport rate (J_{max}). (a) A_{mass}–V_{cmax}, (b) A_{mass}–g_m, (c) V_{cmax}–J_{max}, and (d) g_m–V_{cmax}. The black line was the regression of standard major analysis (SMA) fit to all data in the four phyla (LES SMA) and the other lines were SMA regressions fit to all data of each phylum. The r^2 and slope values were annotated for the LES SMA regression.

The A_{mass} was strongly regulated by V_{cmax} which was in turn related to P_R (LES SMA r^2 = 0.62). Onoda *et al*. (2017) suggested that DeltaC may be an important factor influencing PNUE variations in seed plants. Hence, PNUE correlations with P_R, g_m, and DeltaC were quantified in Fig. 3. We found strong correlation strength between PNUE and P_R across the four phyla (r^2 = 0.45, Fig. 3a). The PNUE–g_m correlation had a higher r^2 (0.52, Fig. 3c) than that with P_R. Path analysis indicated that the two traits explained about 65% of PNUE variations. There was no obvious correlation between PNUE and DeltaC across the four phyla (r^2 = 0.04, Fig. 3c). The

r^2 value was relatively lower for the P_R–g_m relationship (r^2 = 0.20, Fig. 3d), suggesting a weak correlation between them.

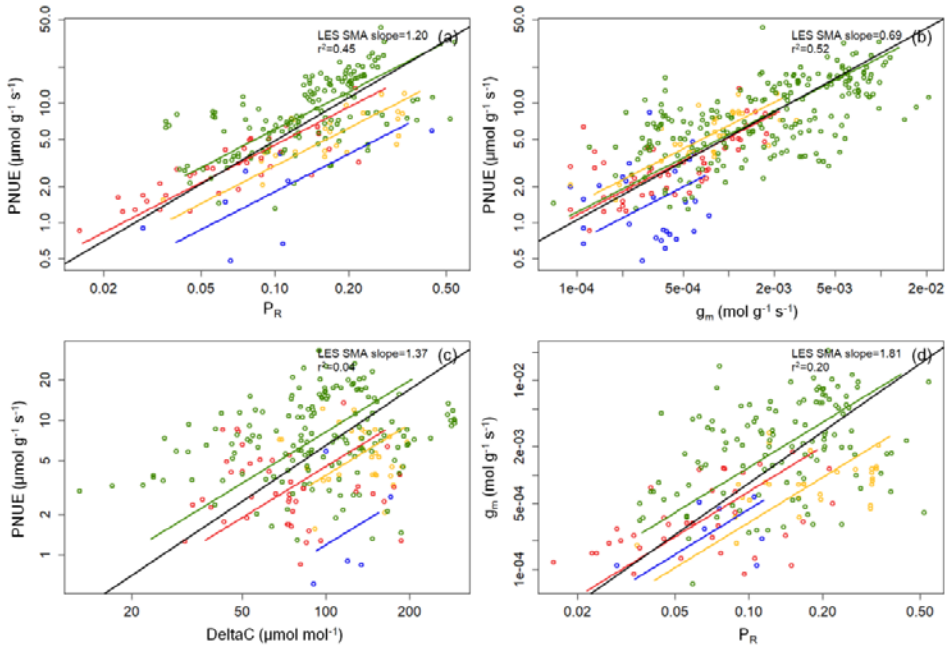

Fig. 3. Paired-trait correlations between the photosynthetic N-use efficiency (PNUE), allocation fraction of leaf nitrogen to Rubisco (P_R), mass-based mesophyll conductance (g_m), internal CO_2 drawdown (DeltaC). (a) PNUE–P_R, (b) PNUE–g_m, (c) PNUE–DeltaC, (d) P_R–g_m. The black line was the regression of standard major analysis (SMA) fit to all data in the four phyla (LES SMA) and the other lines were SMA regressions fit to all data of each phylum. The r^2 and slope values were annotated for the LES SMA regression.

The relative importance of P_R and g_m in determining PNUE is shown in Fig. 4. The PNUE predictions corresponded to observations well at the low- and high-g_m species assembles (Fig. 4a). A close correspondence between PNUE predictions and observations was also observed in most sampled species (Fig. S2). In the high-g_m species assemble (0.25–0.32 mol m^{-2} s^{-1}), the slope of the PNUE–P_R relationship was 57.58, and it was 20.52 for the low-g_m species assemble (0.05–0.06 mol m^{-2} s^{-1}). It suggested that for species with high g_m, a 0.1-unit increase in P_R contributed to a 5.8-unit increase in PNUE, whereas the increment of PNUE was only 2.1-unit in low-g_m species. An exponential decay tendency in l_m-l_b with g_m was observed in all sampled species (Fig. 4b). The l_m overweighed l_b in species with low g_m < 0.001 mol g^{-1} s^{-1} (ca. 0.08 mol m^{-2} s^{-1}), suggesting stronger mesophyll limitation on photosynthesis; *vice verse*, stronger biochemical limitation on photosynthesis was evident in species with high g_m > 0.001 mol g^{-1} s^{-1}. These results suggested stronger limitation by g_m on

PNUE for species with low g_m and stronger limitation by P_R on PNUE in species with high g_m.

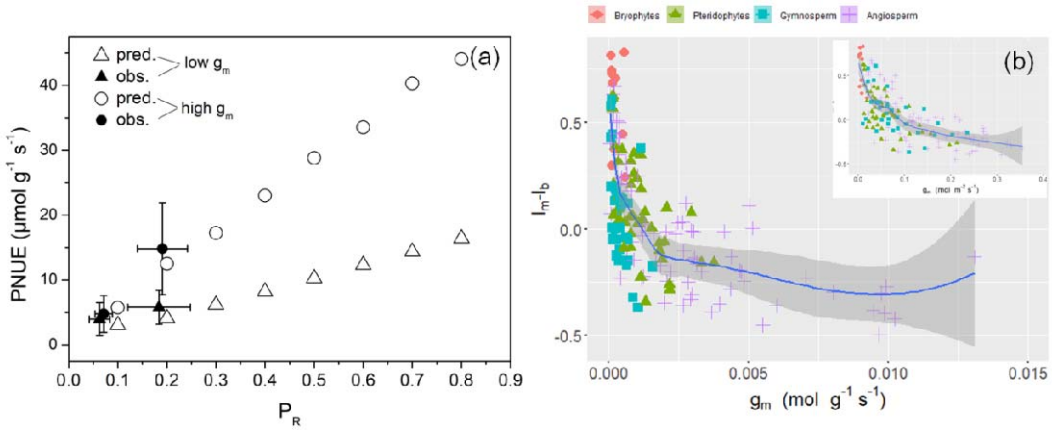

Fig. 4. Model simulations and observations of photosynthetic N-use efficiency (PNUE) at a continuous series of Rubisco nitrogen allocation fraction (P_R) and at two assembles of mesophyll conductance (g_m): high and low ranges (circles and triangles, respectively) in subplot a. Subplot b showed the relationship between l_m-l_b and mass- and area-based g_m. The high-g_m species assemble had g_m range from 0.25 to 0.32 mol m^{-2} s^{-1} and 0.05–0.06 mol m^{-2} s^{-1} in the low-g_m species assemble, corresponding to chloroplast CO_2 concentration (C_c) at about 100 and 230 μmol mol^{-1} under current atmospheric CO_2 condition, respectively. pred.: predictions; obs.: observations; l_m-l_b: the difference between mesophyll conductance limitation and biochemical limitation.

Relationships between morpho-anatomical traits and P_R and g_m

Relationships between morpho-anatomical traits and P_R and g_m are shown in Fig. 5. The P_R had a weak correlation with LMA across the four phyla (r^2 = 0.19, Fig. 5a) and the weak correlation was also observed for g_m and LMA (r^2 = 0.24, Fig. 5b) Statistical results in comparison between Onoda P_R chemical assay dataset and the P_R numerical calculations in spermatophyte showed no significant differences in SMA slope and intercept (p = 0.1, Fig. S3), suggesting that incorporation of the P_R numerical calculations into Onoda P_R chemical assay dataset did not bring systematic biases in trait correlation analysis, and the P_R mixture dataset was reliable. For g_m and T_{cwm}, a consistent relationship with high correlation strength was observed across the four phyla (r^2 = 0.44, Fig. 5c). The g_m in four phyla tended to converge towards the Loess regression line (insert in Fig. 5c). A rapid decline in g_m with T_{cwm} was seen, and g_m tended to level off at higher T_{cwm}. A strong correlation was observed between g_m and the mass-based S_c (r^2 = 0.66, Fig. 5d). Other anatomical traits did not show significant correlations with g_m (r^2 < 0.1, Figs. S4a–f). The P_R was inversely proportional to T_{cwm} with a medium r^2 = 0.30 (Fig. 5e). The DeltaC increased with

increasing T_{cwm}, while their correlation strength was weak (r^2 = 0.14, Fig. 5f), suggesting marginal effects of T_{cwm} on the internal CO_2 drawdown.

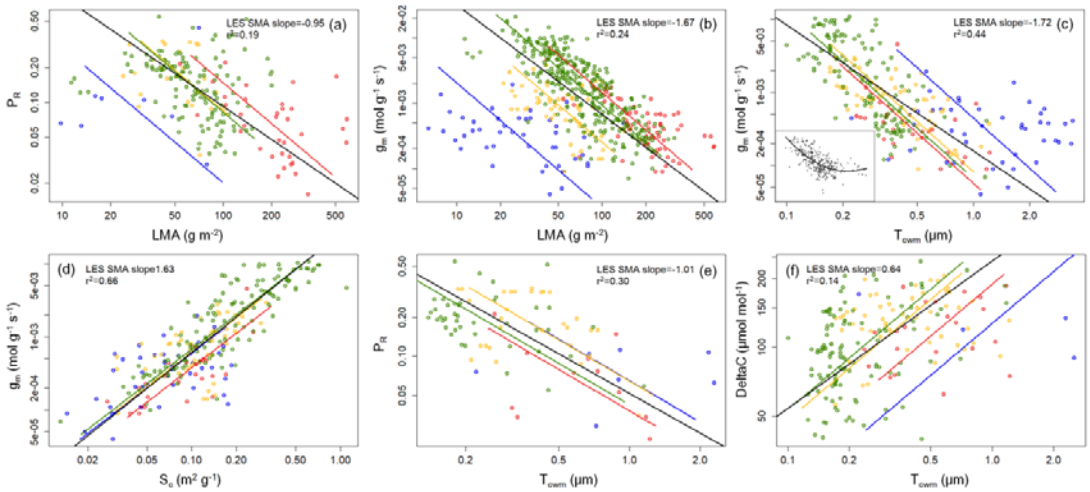

Fig. 5. Paired-trait correlations between allocation fraction of leaf nitrogen to Rubisco (P_R), leaf mass per area (LMA), mesophyll conductance (g_m), mesophyll cell wall thickness (T_{cwm}), chloroplast surface exposed to intercellular airspace area per unit leaf mass (S_c), internal CO_2 drawdown (DeltaC). (a) P_R–LMA, (b) g_m–LMA, (c) g_m–T_{cwm}, (d) g_m–S_c, (e) P_R–T_{cwm}, (f) DeltaC–T_{cwm}. The black line was the regression of standard major analysis (SMA) fit to all data in the four phyla (LES SMA) and the other lines were SMA regressions fit to all data of each phylum. The r^2 and slope values were annotated for the LES SMA regression. The inset in subplot c showed the Loess model fit to the g_m–T_{cwm} correlation.

Path analysis for leaf morpho-anatomical and physiological traits and PNUE

Path analysis for the SEM fit indicated that the seven traits g_m, P_R, LMA, T_{cwm}, mass-based S_c, C_i, and C_c together explained 88% of PNUE variations, and 65% of PNUE variations were interpreted by P_R and g_m (CFI = 1.0, SRMR = 0.02, p = 0.001, Fig. 6a). The traits used for path analysis was chosen primarily according to the aforementioned paired-trait correlation analysis and Eqn 3 parameters. The absolute value of path coefficient (*Q*) for T_{cwm}–g_m was 0.84, which was higher by 13.5% than that for LMA–g_m. The S_c–g_m had a high *Q* = 0.89, confirming their positive correlation shown in Fig. 5d. A higher *Q* value of 27.5% was found in the T_{cwm}–P_R as compared to the LMA–P_R. The *Q* values for P_R–C_i or P_R–C_c were less than 0.3, suggesting low impacts of leaf internal CO_2 concentration on P_R changes across species. The P_R and g_m had direct and substantial impacts on PNUE (*Q* > 0.45), while direct impacts on PNUE by T_{cwm} and LMA were much weaker (*Q* = 0.1 and 0.25, respectively). The phylogenic pattern of T_{cwm} across four phylum groups and the paired-trait correlation for PNUE–T_{cwm} are shown in Figs. 6b and c. A trend of

consistent decline in T_{cwm} from bryophytes to angiosperm was observed. The PNUE was negatively proportional to T_{cwm} with r^2 as high as 0.61, which was higher by five-fold than the PNUE–LMA relationship shown in Fig. 1c. Results suggested that P_R and g_m variations across the four phyla and through plant phylogeny were primarily related to T_{cwm}. Impacts of T_{cwm} on PNUE were achieved through its controls on P_R and g_m.

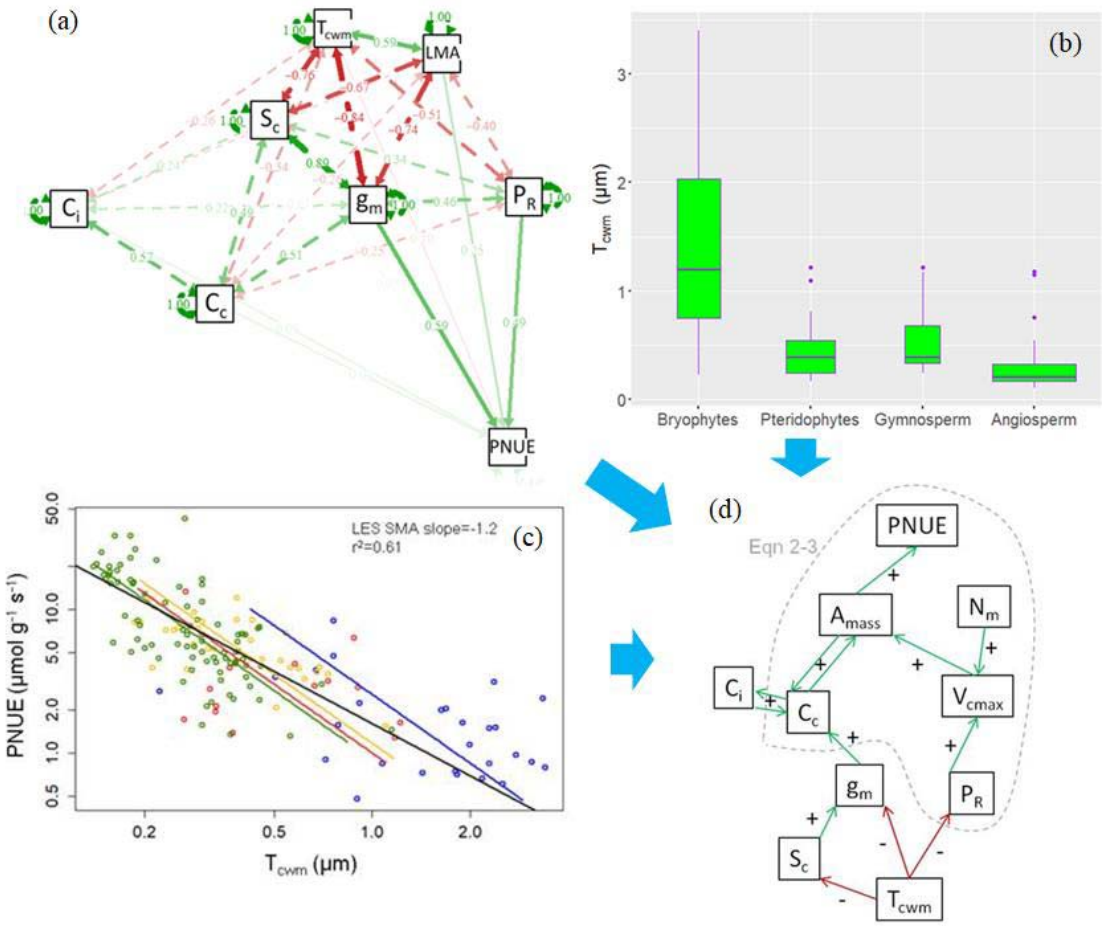

Fig. 6. (a) The circle layout of the path diagram that indicates relationships and the causal direction between PNUE and morpho-physiological traits, (b) the phylogenetic patterns of mesophyll cell wall thickness (T_{cwm}), (c) the paired-trait correlation between photosynthetic-N use efficiency (PNUE) and T_{cwm}, and (d) the structural diagram about T_{cwm}-mediated physiological mechanisms controlling PNUE variations. The arrow and value between each trait and PNUE indicate the path coefficient in subplot a. The boxes were drawn with widths proportional to the square-roots of the number of observations in the phyla in subplot b. The black line was the regression of standard major analysis (SMA) fit to all data in the four phyla (LES SMA) and the other lines were SMA regressions fit to all data of each phylum in subplot c. The r^2 and slope values were annotated for the LES SMA regression. Interrelationships between PNUE and leaf traits embedded by the gray dashed circle in subplot d were deduced according to Eqn 2–3. The "+" and "-" signs reflected positive and negative relations, respectively. P_R: allocation fraction of leaf nitrogen to Rubisco; LMA: leaf

mass per area; g_m: mass-based mesophyll conductance; T_{cwm}: mesophyll cell wall thickness; S_c: chloroplast surface area exposed to intercellular airspace per unit leaf mass; C_i and C_c: leaf intercellular and chloroplastic CO_2 concentration, respectively.

Discussion

Results with causal correlations between leaf traits and PNUE were visualized in Fig. 6c. According to Eqn 2–3, A_{mass} was determined by C_c and V_{cmax}, which in turn were primarily related to C_i and g_m, P_R and N_m, respectively. Increment of N_m contributed to V_{cmax} and then A_{mass}, while its contributions to PNUE were not significant (Fig. S1). In fact, A_{mass} and N_m was positively correlated (LES SMA r^2 = 0.34). It implied that coordinating g_m, C_i and P_R to maximize A_{mass} per unit of leaf nitrogen was prior biological strategy adopted by plants to obtain high PNUE. Previous studies reported conservative C_i values in species grown under non-stress conditions (von Caemmerer and Farquhar, 1981; Evans *et al*., 2009). The coefficient of variation (CV) for C_i in the global database was 0.15, which was much lower than the CV of C_c (0.31). It might be reasonable to infer the critical roles of g_m rather than g_{sw} in determination of C_c in non-stressed plant species (Ethier and Livingston, 2004; Tosens *et al*., 2012; Onoda *et al*., 2017). Bryophytes have thick cell walls and no stomatal conductance structure. Collectively, it's better to choose common leaf traits as bio-indicators to explore PNUE variations along terrestrial plant phylogeny. Cell walls (CWs) have a well recognized importance in plant physiology and biotechnology, and recent reviews suggested that T_{cwm} can be crucial in regulating photosynthesis (Flexas and Carriquí, 2020; Flexas *et al*., 2021). In the paragraphs that followed, T_{cwm}-mediated physiological mechanisms controlling PNUE variations through land plant phylogeny are discussed.

The P_R and g_m are considered two important factors underlying PNUE variations in seed plants (Hikosaka, 2004; Onoda *et al*., 2017). 65% of PNUE variations are explained by the two variables. Our results documented the synergetic effects of the two variables on PNUE across plant phylogeny, namely an increase in either of them could contribute to the improvement of PNUE. However, the synergetic effect of P_R is related to g_m. Increasing P_R contributes to a slight improvement in PNUE in species with low g_m, whereas a double increment in PNUE is achieved in high-g_m species (Fig. 4a). CO_2 enrichments inside chloroplasts due to high g_m facilitate photosynthesis and then a significant increment in PNUE is anticipated. Warren and Adams (2006) suggested that variation in the g_m–photosynthesis relationship contributes to variation

in PNUE. Their suggestion is supported and further explained by our results that photosynthesis is strongly limited by g_m in species with low $g_m < 0.001$ mol g^{-1} s^{-1} (Fig. 4b); *vice versa*, the biochemical limitation is a major factor constraining photosynthesis in high-g_m species. Greater improvement in PNUE is achieved in high-g_m species than the low-g_m species in condition of the same P_R. The g_m threshold where the relative importance of P_R and g_m in determining PNUE shifts emerges at 0.001 mol g^{-1} s^{-1}, corresponding to the area-based g_m from 0.05 to 0.1 mol m^{-2} s^{-1}. Covariance in A_{mass}, g_m, and Rubisco content in hundreds of rice varieties were evaluated by Xiong and Flexas (2018), reporting low g_m limitation and strong Rubisco limitation in modern varieties. PNUE improvement in modern varieties would be further facilitated by the improvement of Rubisco carboxylation capacity. A pronounced increment in PNUE would be possible in high-g_m species via efforts to ameliorate carboxylation efficiency. Collectively, PNUE variations across major plant groups are strongly regulated by P_R and g_m, and the P_R effects on PNUE are species-dependent on g_m.

The g_m is a composite conductance of the CO_2 diffusion pathway between the substomatal cavities and the sites of carboxylation within chloroplasts. Previous studies highlighted the importance of cell wall composition (Ellsworth *et al*., 2018; Carriquí *et al*., 2020; Roig-Oliver *et al*., 2021), cell wall porosity (Evans *et al*., 2009), cell wall thickness (Carriquí *et al*., 2015, 2019, 2021; Flexas *et al*., 2021), chloroplast distribution, in particular the S_c (Carriquí *et al*., 2015, 2019; Tosens *et al*., 2016; Han *et al*., 2018; Du *et al*., 2019; Ren *et al*., 2019; Nadal *et al*., 2021), in determining g_m. Our results suggested strong and positive correlation between g_m and S_c, while significantly negative relationship between g_m and T_{cwm} across major plant groups and through phylogeny (Figs. 5c and d; Fig. 6a). There is an exponential decay tendency in g_m with increasing T_{cwm}, and the low g_m value tends to level off at greater T_{cwm} (Fig. S5), implying that species with thicker cell walls may have the same g_m as compared to those with relatively thin cell walls. As reported in resurrection plants with thick T_{cwm} by Nadal *et al*. (2021), greater S_c could compensate for thick cell wall limitation to obtain relatively high g_m. A large range of g_m at given T_{cwm} in Fig. 5c mainly arises from differences in S_c among species. Negative correlation between S_c and T_{cwm} were observed across major plant groups, suggesting higher S_c at the low-end of T_{cwm} axis along plant phylogeny. Optimal arrangement of chloroplast position along cell walls

could minimize CO_2 diffusion resistance at liquid phase and enlarge diffusion area of CO_2, contributing to g_m.

A negative P_R–LMA relationship in regional vegetation was reported by Luo *et al*. (2021). In line with their reports, the P_R is inversely scaled with LMA (Fig. 5a), and the relationship is analogous to the g_m–T_{cwm} relationship. There is a progressive phylogenetic trend associated with LMA and T_{cwm} in spermatophyta: from low LMA and thin T_{cwm} in angiosperms to high LMA and great T_{cwm} in gymnosperm (Onoda *et al*., 2017; Flexas *et al*., 2021; Xing *et al*., 2021), while an exception occurred in mosses and ferns that have low LMA (Tosens *et al*., 2016; Carriquí *et al*., 2019). Interestingly, a consistent phylogenetic trend regarding T_{cwm} from bryophytes to angiosperm is reported in the study of Gago *et al*. (2019) and in Fig. 6b in our study: from very large T_{cwm} in bryophytes to very low T_{cwm} in angiosperms. Higher correlation strength is indeed achieved when scaling g_m with T_{cwm} as compared to that for g_m–LMA (Figs. 5b and c and Fig. 6a). The log-transformed g_m–T_{cwm} relationship exhibits more convergent characteristics in g_m changes with T_{cwm} (i.e., g_m coming closer together at given T_{cwm}). It suggested that the P_R–T_{cwm} relationship is likely synonymous with the exponential decay correlation of P_R–LMA, or at least it should be. Theoretical predictions by Evans *et al.* (2009) suggested that other elements in the mesophyll CO_2 diffusion pathway of the liquid phase could co-vary with T_{cwm}, such as a decline in Rubisco per unit of exposed chloroplast surface area and thinner chloroplast with increasing T_{cwm}. If the P_R, which is proportional to photosynthesis, did not decrease with increases in T_{cwm}, then the CO_2 drawdown "DeltaC" would have been much greater than observations. If the g_m decreased by ten folds due to increasing T_{cwm} from 0.2 to 0.5 μm (e.g., the g_m decline from 0.004 to 0.0004 mol g^{-1} s^{-1}), then cell wall thickness 0.5 μm would increase CO_2 drawdown by more than five folds, and strong correlation between DeltaC and T_{cwm} would therefore be observed. However, this expectation contradicts the fact that the actual increment of CO_2 drawdown is limited to 50% (Fig. 5f). The net result of the decline in P_R with T_{cwm} is to balance the increase in mesophyll resistance so that the CO_2 drawdown is only weakly proportional to T_{cwm} (Fig. 5f). The theoretical prediction regarding the T_{cwm}–biochemical capacity offset mechanisms in the study of Evans *et al*. (2009) is supported by experimental results in this study, i.e., a significantly negative correlation between T_{cwm} and P_R (Fig. 5e and Fig. 6a). In our study, the observed significance of T_{cwm}–P_R negative correlation across major plant groups is aligned with

the founding in seed plants in the study of Onoda *et al*. (2017). However, the predicted inverse correlation between chloroplast thickness and T_{cwm} is not observed (Fig. S6). One of the distinctive differences in leaf anatomy among bryophytes, ferns, and spermatophytes is the thickness of photosynthetic tissues (Han *et al*., 2018; Carriquí *et al*., 2019). The T_{cwm}-induced decline in P_R may result in the decline of chloroplast amount per leaf mass. An open question rises regarding whether the response pattern of P_R to T_{cwm} is exclusively independent or dependent causality of g_m changes. The possibility of g_m effects on the observed P_R–T_{cwm} response pattern could be excluded because no strong correlation is observed for either P_R–g_m relationship (Fig. 3d) or V_{cmax}–C_c relationship (Fig. S7). Concerning the generality of significant correlations for P_R–T_{cwm} and g_m–T_{cwm} in the global database, it suggested that T_{cwm} is the critical factor controlling evolutionary changes of PNUE from bryophytes to angiosperm.

Results in this study help understand the complex morpho-physiological mechanisms shaping PNUE variations along land plant phylogeny. Theoretical predictions and statistical analysis suggested that P_R and g_m concurrently contribute to inter-specific PNUE variations, whereas P_R effects are strongly dependent on g_m. Improvement of PNUE in high-g_m species due to increasing P_R is much higher than that in low-g_m species. The g_m is positively and negatively related to S_c and T_{cwm}, respectively. Negative correlations for P_R–T_{cwm} and S_c–T_{cwm} were observed. Coordinating changes in P_R and g_m connecting T_{cwm} ensures that the internal CO_2 drawdown is relatively conservative over a large range of T_{cwm}. Effects of T_{cwm} on PNUE are achieved through its controls on g_m and P_R. T_{cwm} could be a viable predictor to help explore the evolutional trajectory of plant PNUE.

Acknowledgments

This work was supported by the National Natural Science Foundation of China (32001129) and Estonian Research Council (PUT 1473).

Author contributions:

Conceptualization: DDL, WX

Methodology, supervision, and visualization: WX

Investigation: DDL, WX

Writing—original draft: DDL, WX

Writing—review & editing: MC, DLX, TT, WX

Competing interests: Authors declare that they have no competing interests.

Data and materials availability: All data are available in the supplementary materials.

References

Anderegg L D L, Berner L T, Badgley G, Sethi M L, Law B E, HilleRisLambers J. 2018. Within-species patterns challenge our understanding of the leaf economics spectrum. Ecology Letters 21, 734-744.

Bahar N H A, Hayes L, Scafaro A P, Atkin O K, Evans J R. 2018. Mesophyll conductance does not contribute to greater photosynthetic rate per unit nitrogen in temperate compared with tropical evergreen wet-forest tree leaves. New Phytologist 218, 492-505.

Bernacchi C J, Portis A R, Nakano H, von Caemmerer S, Long S P. 2002. Temperature response of mesophyll conductance. Implications for the determination of Rubisco enzyme kinetics and for limitations to photosynthesis in vivo. Plant Physiology 130, 1992-1998.

Carriquí M, Cabrera H M, Conesa M À, Coopman R E, Douthe C, Gago J, Gallé A, Galmés J, Ribas-Carbo M, Tomás M et al. 2015. Diffusional limitations explain the lower photosynthetic capacity of ferns as compared with angiosperms in a common garden study. Plant, Cell & Environment 38, 448-460.

Carriquí M, Roig-Oliver M, Brodribb T J, Coopman R, Gill W, Mark K, Niinemets Ü, Perera-Castro A V, Ribas-Carbó M, Sack L et al. 2019. Anatomical constraints to nonstomatal diffusion conductance and photosynthesis in lycophytes and bryophytes. New Phytologist 222, 1256-1270.

Carriquí M, Nadal M, Clemente-Moreno MJ, Gago J, Miedes E, Flexas J. 2020. Cell wall composition strongly influences mesophyll conductance in gymnosperms. The Plant Journal 103, 1372-1385.

Carriquí M, Nadal M, Flexas J. 2021. Acclimation of mesophyll conductance and anatomy to light during leaf aging in *Arabidopsis thaliana*. Physiologia Plantarum 172, 1894-1907.

Du Q J, Liu T, Jiao X, Song X M, Zhang J Y, Li J M. 2019. Leaf anatomical adaptations have central roles in photosynthetic acclimation to humidity. Journal of Experimental Botany 70, 4949-4961.

Ellsworth P V, Ellsworth P Z, Koteyeva N K, Cousins A B. 2018. Cell wall properties in *Oryza sativa* influence mesophyll CO_2 conductance. New Phytologist 219, 66-76.

Ethier G J, Livingston N J. 2004. On the need to incorporate sensitivity to CO_2 transfer conductance into the Farquhar–von Caemmerer–Berry leaf photosynthesis model. Plant, Cell & Environment 27, 137-153.

Evans J R, Kaldenhoff R, Genty B, Terashima I. 2009. Resistances along the CO_2 diffusion pathway inside leaves. Journal of Experimental Botany 60, 2235-2248.

Evans J R. 2021. Mesophyll conductance: walls, membranes and spatial complexity. New Phytologist 229, 1864-1876.

Farquhar G D, von Caemmerer S, Ball J A. 1980. A biochemical model of photosynthetic CO_2 assimilation in leaves of C_3 species. Planta 149, 78-90.

Flexas J, Carriquí M. 2020. Photosynthesis and photosynthetic efficiencies along the terrestrial plant's phylogeny: lessons for improving crop photosynthesis. The Plant Journal 101, 964-978.

Flexas J, Clemente-Moreno M J, Bota J, Brodribb T J, Gago J, Mizokami Y, Nadal M, Perera-Castro A V, Roig-Oliver M, Sugiura D et al. 2021. Cell wall thickness and composition are involved in photosynthetic limitation. Journal of Experimental Botany 72, 3971-3986.

Gago J, Carriquí M, Nadal M, Clemente-Moreno M J, Coopman R E, Fernie A R, Flexas J. 2019. Photosynthesis optimized across land plant phylogeny. Trends in Plant Science 24, 947-958.

Garnier E, Gobin O, Poorter H. 1995. Nitrogen productivity depends on photosynthetic nitrogen use efficiency and on nitrogen allocation within the plant. Annals of Botany 76, 667-672.

Gómez-Ocampo G, Ploschuk E L, Mantese A, Crocco C D, Botto J F. 2021. BBX21 reduces abscisic acid sensitivity, mesophyll conductance and chloroplast electron transport capacity to increase photosynthesis and water use efficiency in potato plants cultivated under moderated drought. The Plant Journal 108, 1131-1144.

Gvozdevaite A, Oliveras I, Domingues T F, Peprah T, Boakye M, Afriyie L, da Silva Peixoto K, de Farias J, Almeida de Oliveira E, Almeida Farias et al. 2018. Leaf-

level photosynthetic capacity dynamics in relation to soil and foliar nutrients along forest–savanna boundaries in Ghana and Brazil. Tree Physiology 38, 1912-1925.

Han J M, Lei Z Y, Flexas J, Zhang Y J, Carriqui, Zhang W F, Zhang Y L. 2018. Mesophyll conductance in cotton bracts: anatomically determined internal CO_2 diffusion constraints on photosynthesis. Journal of Experimental Botany 69, 5433-5443.

Harrison S P, Cramer W, Franklin O, Prentice I C, Wang H, Brännström Å, de Boer H, Dieckmann U, Joshi J, Keenan T F, Lavergne A. 2021. Eco-evolutionary optimality as a means to improve vegetation and land-surface models. New Phytologist 231, 2125-2141.

Hayes FJ, Buchanan SW, Coleman B, Gordon AM, Reich PB, Thevathasan NV, Wright IJ, Martin AR. 2019. Intraspecific variation in soy across the leaf economics spectrum. Annals of Botany 123, 107-120.

Hidaka A, Kitayama K. 2009. Divergent patterns of photosynthetic phosphorus-use efficiency versus nitrogen-use efficiency of tree leaves along nutrient-availability gradients. Journal of Ecology 97, 984-991.

Hikosaka K, Hanba Y T, Hirose T, Terashima I. 1998. Photosynthetic nitrogen-use efficiency in leaves of woody and herbaceous species. Functional Ecology 12, 896-905.

Hikosaka K. 2004. Interspecific difference in the photosynthesis-nitrogen relationship: patterns, physiological causes, and ecological importance. Journal of Plant Research 117, 481-494.

Hikosaka K. 2010. Mechanisms underlying interspecific variation in photosynthetic capacity across wild plant species. Plant Biotechnology 27, 223-229.

Kaldenhoff R. 2012. Mechanisms underlying CO_2 diffusion in leaves. Current Opinion in Plant Biology 15, 276-281.

Kurmangozhinov A, Xue W, Li X, Zeng F, Sabit R, Tusun T. 2020. High biomass production with abundant leaf litterfall is critical to ameliorating soil quality and productivity in reclaimed sandy desertification land. Journal of Environmental Management 263, 110373.

Lei Z Y, Wang H, Wright I J, Zhu X-G, Niinemets Ü, Li Z-L, Sun D S, Dong N, Zhang W F, Zhou Z L et al. 2021a. Enhanced photosynthetic nitrogen use

efficiency and increased nitrogen allocation to photosynthetic machinery under cotton domestication. Photosynthesis Research 150, 239-250.

Lei Z, Liu F, Wright I J, Carriquí M, Niinemets Ü, Han J, Jia M, Atwell B J, Cai X, Zhang W et al. 2021b. Comparisons of photosynthetic and anatomical traits between wild and domesticated cotton. Journal of Experimental Botany 73, 873-885.

Luo X, Keenan T F, Chen J M, Croft H, Colin Prentice I, Smith N G, Walker A P, Wang H, Wang R, Xu C et al. 2021. Global variation in the fraction of leaf nitrogen allocated to photosynthesis. Nature Communications 12.

Maire V, Martre P, Kattge J, Gastal F, Esser G, Fontaine S, Soussana J F. 2012. The coordination of leaf photosynthesis links C and N fluxes in C_3 plant species. PloS One 7.

Martin AR, Hale CE, Cerabolini BEL, Cornelissen JHC, Craine J, Gough WA, Kattge J, Tirona CKF. 2018. Inter- and intraspecific variation in leaf economic traits in wheat and maize. AoB Plants, 10, ply006.

Medlyn B E, Dreyer E, Ellsworth D, Forstreuter M, Harley P C, Kirschbaum M U F, Le Roux X, Montpied P, Strassemeyer J, Walcroft A. 2002. Temperature response of parameters of a biochemically based model of photosynthesis. II. A review of experimental data. Plant, Cell & Environment 25, 1167-1179.

Nadal M, Perera-Castro A V, Gulías J, Farrant J M, Flexas J. 2021. Resurrection plants optimize photosynthesis despite very thick cell walls by means of chloroplast distribution. Journal of Experimental Botany 72, 2600-2610.

Niinemets Ü, Tenhunen J D. 1997. A model separating leaf structural and physiological effects on carbon gain along light gradients for the shade-tolerant species Acer saccharum. Plant, Cell & Environment 20, 845-866.

Oguchi R, Ozaki H, Hanada K, Hikosaka K. 2016. Which plant trait explains the variations in relative growth rate and its response to elevated carbon dioxide concentration among Arabidopsis thaliana ecotypes derived from a variety of habitats? Oecologia 180, 865-876.

Onoda Y, Hikosaka K, Hirose T. 2004. Allocation of nitrogen to cell walls decreases photosynthetic nitrogen-use efficiency. Functional Ecology 18, 419-425.

Onoda Y, Wright I J, Evans J R, Hikosaka K, Kitajima K, Niinemets Ü, Poorter H, Tosens T, Westoby M. 2017. Physiological and structural tradeoffs underlying the leaf economics spectrum. New Phytologist 214, 1447-1463.

Popper, Z A, Fry S, 2003. Primary cell wall composition of bryophytes and charophytes. Annals of Botany 91, 1-12.

Preston C D, Hill MO. 1999. The geographical relationships of the British and Irish flora: a comparison of pteridophytes, flowering plants, liverworts and mosses. Journal of Biogeography 26, 629-642.

Pons T L, Westbeek M H M. 2004. Analysis of differences in photosynthetic nitrogen-use efficiency between four contrasting species. Physiologia Plantarum 122, 68-78.

Poorter H, Evans J R. 1998. Photosynthetic nitrogen-use efficiency of species that differ inherently in specific leaf area. Oecologia 116, 26-37.

Poorter H, Niinemets Ü, Poorter L, Wright I J, Villar R. 2009. Causes and consequences of variation in leaf mass per area (LMA): a meta-analysis. New Phytologist 182, 565-588.

Poorter H, Remkes C, Lambers H. 1990. Carbon and nitrogen economy of 24 wild species differing in relative growth rate. Plant Physiology 94, 621-627.

Popper Z A, Michel G, Herve C, Domozych D S, Willats W G T, Tuohy M G, Kloareg B, Stengel D B. 2011. Evolution and diversity of plant cell walls: From algae to flowering plants. In: Merchant, S.S., Briggs, W.R., Ort, D. (Eds.), Annual Review of Plant Biology, Vol 62, pp. 567.

R Core Team. 2021. R: A Language and Environment for Statistical Computing; R Foundation for Statistical Computing: Vienna, Austria, Available online: https://www.R-project.org/ (accessed on May 2022).

Reich P B, Ellsworth D S, Walters M B. 1998. Leaf structure (specific leaf area) modulates photosynthesis-nitrogen relations: evidence from within and across species and functional groups. Functional Ecology 12, 948-958.

Ren T, Weraduwage S M, Sharkey T D. 2019. Prospects for enhancing leaf photosynthetic capacity by manipulating mesophyll cell morphology. Journal of Experimental Botany 70, 1153-1165.

Ripullone F, Grassi G, Lauteri M, Borghetti M. 2003. Photosynthesis–nitrogen relationships: interpretation of different patterns between Pseudotsuga menziesii and Populus × euroamericana in a mini-stand experiment. Tree Physiology 23, 137-144.

Roig-Oliver M, Douthe C, Bota J, Flexas J. 2021. Cell wall thickness and composition are related to photosynthesis in Antarctic mosses. Physiologia Plantarum 173, 1914-1925.

Rosseel Y. 2012. Lavaan: an R package for structural equation modeling. Journal of Statistical Software 48, 1-36.

Sharkey T.D., Bernacchi C.J., Farquhar G.D., Singsaas E.L., 2007. Fitting photosynthetic carbon dioxide response curves for C_3 leaves. Plant Cell and Environment 30, 1035–1040.

Shipley B, Lechowicz M J, Wright I, Reich P B. 2006. Fundamental trade-offs generating the worldwide leaf economics spectrum. Ecology 87, 535-541.

Shipley B. 2004. Cause and correlation in biology: A user's guide to path analysis, structural equations and causal inference. Cambridge University Press, Cambridge, UK.

Smith N G, Keenan T F, Colin Prentice I, Wang H, Wright I J, Niinemets Ü, Crous K Y, Domingues T F, Guerrieri R, Yoko Ishida F et al. 2019. Global photosynthetic capacity is optimized to the environment. Ecology Letters 22, 506-517.

Takashima T, Hikosaka K, Hirose T. 2004. Photosynthesis or persistence: nitrogen allocation in leaves of evergreen and deciduous Quercus species. Plant Cell and Environment 27, 1047-1054.

Tosens T, Niinemets Ü, Vislap V, Eichelmann H, Castro-Díez P. 2012. Developmental changes in mesophyll diffusion conductance and photosynthetic capacity under different light and water availabilities in Populus tremula: how structure constrains function. Plant, Cell & Environment 35, 839-856.

Tosens T, Nishida K, Gago J, Coopman R E, Cabrera H M, Carriquí M, Laanisto L, Morales L, Nadal M, Rojas R et al. 2016. The photosynthetic capacity in 35 ferns and fern allies: mesophyll CO_2 diffusion as a key trait. New Phytologist 209, 1576-1590.

von Caemmerer S, Farquhar G D. 1981. Some relationships between the biochemistry of photosynthesis and the gas exchange of leaves. Planta 153, 376-387.

von Caemmerer, S., 2020. Rubisco carboxylase/oxygenase: from the enzyme to the globe: a gas exchange perspective. Journal of Plant Physiology 252, 153240.

Wang M, Yuan D, Gao W, Li Y, Tan J, Zhang X. 2013. A comparative genome analysis of PME and PMEI families reveals the evolution of pectin metabolism in plant cell walls. Plos One 8.

Wang H, Prentice I C, Keenan T F, Davis T W, Wright I J, Cornwell WK, Evans B J, Peng C. 2017. Towards a universal model for carbon dioxide uptake by plants. Nature Plants 3, 734-741.

Warren C R, Adams M A. 2006. Internal conductance does not scale with photosynthetic capacity: implications for carbon isotope discrimination and the economics of water and nitrogen use in photosynthesis. Plant, Cell & Environment 29, 192-201.

Warren CR, Adams M A. 2000. Trade-offs between the persistence of foliage and productivity in two Pinus species. Oecologia 124, 487-494.

Wright I J, Reich P B, Cornelissen J H C, Falster D S, Garnier E, Hikosaka K, Lamont B B, Lee W, Oleksyn J, Osada N. 2005. Assessing the generality of global leaf trait relationships. New Phytologist 166, 485-496.

Xing K, Niinemets Ü, Rengel Z, Onoda Y, Xia J, Chen H Y H, Zhao M, Han W, Li H. 2021. Global patterns of leaf construction traits and their covariation along climate and soil environmental gradients. New Phytologist 232, 1648-1660.

Xiong D, Flexas J. 2018. Leaf economics spectrum in rice: leaf anatomical, biochemical, and physiological trait trade-offs. Journal of Experimental Botany 69, 5599-5609.

Xue W, Li X, Zeng F. 2021. Inter-annual variations of seed cotton yield in relation to soil organic carbon and harvest index in reclaimed desertified land. Field Crops Research 272, 108267.

Xue W., Luo H., Carriquí M., Nadal M., Huang J.F., Zhang J.L., 2022. Quantitative expression of mesophyll conductance temperature response in the FvCB model and impacts on plant gas exchange estimations. Agricultural and Forest Meteorology 325, 109153.

Yin L J, Xu H C, Dong S X, Chu J P, Dai X L, He M R. 2019. Optimised nitrogen allocation favors improvement in canopy photosynthetic nitrogen-use efficiency: Evidence from late-sown winter wheat. Environmental and Experimental Botany 159, 75-86.